# Demodulation and denoising techniques for a multiplexed fibre fizeau interferometer and fibre bragg grating sensor system based on wavelet analysis

**Author:**
Wong, Allan; Peng, Gang-Ding

**Publication details:**
5th International Conference on Optical Communications and Networks & the 2nd International Symposium on Advances and Trends in Fiber Optics and Applications
pp. 484-487
7811142643 (ISBN)

**Event details:**
5th International Conference on Optical Communications and Networks & the 2nd International Symposium on Advances and Trends in Fiber Optics and Applications
Chengdu & Jiuzhaigou, China

**Publication Date:**
2006

**DOI:**
https://doi.org/10.26190/unsworks/640

# DEMODULATION AND DENOISING TECHNIQUES FOR A MULTIPLEXED FIBRE FIZEAU INTERFEROMETER AND FIBRE BRAGG GRATING SENSOR SYSTEM BASED ON WAVELET ANALYSIS

*Allan C. L. Wong and Gang-Ding Peng**
School of Electrical Engineering and Telecommunications, University of New South Wales, Sydney NSW 2052, Australia

**ABSTRACT**

*Wavelet analysis is applied extensively to a multiplexed fibre Fizeau interferometer and fibre Bragg grating sensor system. Specifically, the discrete wavelet transform is used to demodulate the multiplexed sensor signal simultaneously; and two wavelet denoising methods are used to reduce the noise present in the signal and measurands record. Experimental demonstration is performed through the simultaneous measurement of quasi-static strain and temperature.*

**Keywords:** *Fibre Fizeau interferometer, fibre Bragg grating, wavelet analysis, simultaneous demodulation, noise reduction, strain, temperature*

## 1. INTRODUCTION

### 1.1 Overview

Fibre Fizeau interferometers (FFI) and fibre Bragg gratings (FBG) are two of the widely studied types of fibre-optic sensors. They have distinct properties and advantages that, when combined together, they can measure two different measurands, such as strain and temperature, simultaneously [1]. Previously, much of the research on the simultaneous demodulation of FFI and FBG was done by using interferometric methods [2-3]. The disadvantages are: they need a high precision and a complicated setup for interrogation, have a relatively small measurement range due to phase ambiguities, and suffer from large static phase drift due to environmental effects. Although drift compensation methods have been proposed, the techniques become more involved, and thus increase the total cost of the system.

Here, simultaneous demodulation and denoising techniques for a multiplexed FFI and FBG sensor system are described. The sensor system is multiplexed through a combination of spatial frequency and wavelength division multiplexing, and is interrogated by a passive spectral detection. Discrete wavelet transform (DWT) with signal processing (SP) methods is used to demodulate the multiplexed sensor signal. Wavelet denoising methods, i.e., hard-thresholding (HT) and block-level-thresholding (BLT), are used to denoise the sensor signal and measurands record. As the sensor system does not use interferometric method and external high-frequency moving parts, it is well suited for the simultaneous measurement of long-term quasi-static strain and temperature of structures such as bridges.

*Corresponding author. E-mail: G.Peng@unsw.edu.au

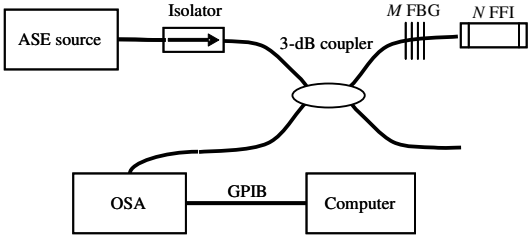


*Fig. 1. Schematic setup of the multiplexed sensor system.*

### 1.2 Sensor system setup

The setup of the sensor system is depicted in Fig. 1. A broadband light source is connected to a 3-dB coupler and is used to illuminate the FFI and FBG sensors. The reflected sensor signal is passed to an optical spectrum analyser (OSA), and is processed by a computer. With this interrogation, the multiplexed sensor signal detected by the OSA is the superposition of the two individual sensor signals. For $N$ FFIs [4] and $M$ FBGs, neglecting high-order and cross-term effects, it is of the form,

$$\begin{aligned} I(\lambda) &= \sum I(\lambda)_{FFI} + \sum I(\lambda)_{FBG} \\ &= A(\lambda)\left\{\sum_{k=1}^{N} r_{1,k} r_{2,k}\left[1 + V_k \cos(4\pi d_k / \lambda)\right], \right. \\ &\quad \left. + \sum_{l=1}^{M} R_{B,l} \exp\left[-(\lambda - \lambda_{B,l})^2 / 2\delta\lambda_{B,l}^2\right]\right\} \end{aligned} \quad (1)$$

where $A(\lambda)$ is the incident light source intensity spectrum, $r_1$ & $r_2$ are the reflection coefficients of the two fibre ends that formed the FFI cavity, $V$ is the fringe visibility, $d$ is the FFI cavity length, $R_B$ is the peak reflectivity of the FBG, $\lambda_B$ is the Bragg wavelength, and $\delta\lambda_B$ is a parameter related to the FBG bandwidth. The FBG sensor signal is approximated from the measured reflection spectrum.

## 2. DEMODULATION AND DENOISING TECHNIQUES

### 2.1 Demodulation algorithm

The demodulation algorithm of this sensor system is depicted in Fig. 2. Detail descriptions of certain crucial

steps are given in following subsections. The raw signal acquired from the OSA is noisy due to fluctuations of light source, and inherit defects and coupling conditions of the sensors. The raw signal is first denoised using the HT wavelet denoising. Then, the DWT is applied to demodulate the FFIs and FBGs. The DWT approximation and detail coefficients are processed separately and simultaneously, in which some SP methods are applied to determinate their measurand-induced physical changes. By employing the DWT in the demodulation, the BLT wavelet denoising is applied automatically to further reduce the noise of the signal. As the physical changes are determined, two different measurands can be detected and recorded. The recorded measurands data usually contain noises, therefore, HT denoising can be applied again to reduce the noise.

**2.2 Multiresolution analysis**

The demodulation technique is based on the theory of multiresolution analysis [5] of the DWT. In this approach, a signal can be represented as:

$$f(t) = \sum_m c_J(m)\phi_{J,m}(t) + \sum_m \sum_{j=1}^{J} d_j(m)\psi_{j,m}(t), \quad (2)$$

where $j, m \in Z$, and the integer $J$ sets the highest decomposition level. $c_j(m)$ are the $j$th-level DWT approximation coefficients, and $d_j(m)$ are the $j$th-level DWT detail coefficients. $\phi_{j,m}(m)$ is the scaling function, and $\psi_{j,m}(m)$ is the wavelet function.

The DWT coefficients can be computed by a multistage two-channel quadrature mirror filter bank (QMFB). This is formed by the scaling function that acts as a low-pass filter, $\phi(t) = \sum_m h(m)\sqrt{2}\phi(2t-m)$, where $m \in Z$ and $h$ are the low-pass filter coefficients. The complementary wavelet function acts as a high-pass filter, $\psi(t) = \sum_m g(m)\sqrt{2}\phi(2t-m)$, where $g$ are the high-pass filter coefficients. At the $j$th-stage of the QMFB, the DWT approximation coefficients are given by $A_j = c_j(m) = \sum_k h(k-2m)c_{j-1}(k)$, and the DWT detail coefficients are given by, $D_j = d_j(m) = \sum_k g(k-2m)c_{j-1}(k)$. This shows that the $j$th-level DWT coefficients are computed by convolving the QMFB with the $(j-1)$th-level approximation coefficients, i.e., $A_{j-1} = A_j + D_j$. By repeating this decomposition in cascade using the most recent $A_j$ as the inputs, we can compute the DWT coefficients to the resolution level of interest, and the signal can be effectively expressed as,

$$f(t) = \sum_m A_J + \sum_m \sum_{j=1}^{J} D_j. \quad (3)$$

**2.3 Signal demodulation**

Having established the principle of the demodulation technique, we now apply the DWT to decompose the sensor signal into multilevel DWT coefficients. A Meyer wavelet is used. First, the $\lambda_B$-shift of the FBG is determined. The received signal is a function of wavelength, thus, the $\lambda_B$ can be determined directly from the 3rd-level approximation coefficients, which give the noise-reduced version of the original wavelength spectrum. By taking the approximation coefficients at this level, it applies the BLT wavelet denoising automatically to reduce the noise. This denoising method is described in the next subsection. After that, an interpolation method is applied around the $\lambda_B$-peak to increase the resolution. By knowing the $\lambda_B$-shift, the measurands change can be detected.

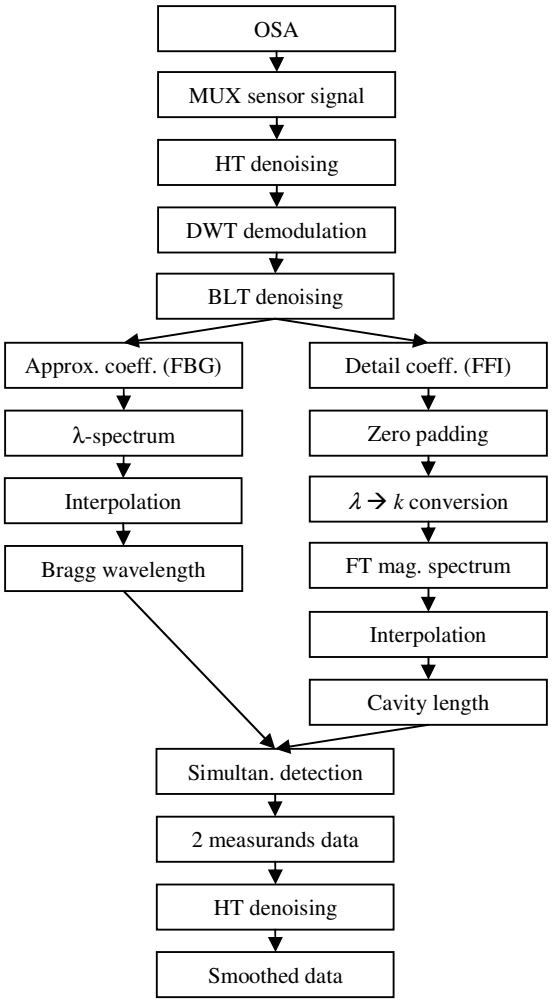


*Fig. 2. Demodulation algorithm.*

Next, the $d$ change of the FFI is determined. We obtain the detail coefficients by taking the DWT of the sensor signal, which is the mean-removed interference pattern of the FFI. The actual level of detail coefficients depends on the spatial frequency of the sensor, which is related to $d$. For example, a longer $d$ produces a signal with a higher spatial frequency. The interference pattern is then demodulated by employing the Fourier transform (FT) peak detection. First, the detail coefficients are converted to a function of wavenumber, so that the FT

variable is directly related to $d$ of the sensor. The $d$ can be obtained directly from the location of the amplitude peak in the FT magnitude spectrum. Next, we increase the resolution by reducing the sampling interval width of the magnitude spectrum. This can be done by applying zero padding to the detail coefficients before taking the FT. The sampling interval width can be further reduced by applying an interpolation method around the FT amplitude peak. By knowing the $d$ change, the measurands change can be detected.

### 2.4 Wavelet denoising methods

Two wavelet denoising methods are employed in the demodulation algorithm: HT and BLT. In HT [6], a signal represented by Eq. (2) is decomposed into wavelet coefficients using the DWT with a 4th-order Daubechies wavelet. A threshold value $h$ is applied to the detail coefficients $d_{ij}$, where most of noise components are present. Any coefficients below $h$ are suppressed, while those above $h$ are kept, i.e.,

$$d'_{i,j} = \xi_h[d_{i,j}] = \begin{cases} d_{i,j}, & |d_{i,j}| > h \\ 0, & |d_{i,j}| \le h \end{cases}. \qquad (4)$$

Then, the denoised signal is reconstructed by taking the inverse DWT. $h$ is empirically chosen such that it can eliminate most noises while retaining the signal features. HT is applied to the raw sensor signal and the recorded measurands data.

BLT is a modified version of the block-thresholding method [7], in which a thresholding rule is applied to a block of coefficients rather than to each coefficient individually. The BLT is modified to set an entire level of coefficients as a block, and apply a rule either to retain and shrink, or to kill the coefficients. The main advantage of using BLT is that it is applied automatically through the demodulation technique.

## 3. SIMULTANEOUS MEASUREMENT

Once the physical changes of both FFI and FBG are known using the above demodulation algorithm, simultaneous measurement of two measurands, such as ε and T, can be performed. We solve two linear equations,

$$\begin{aligned} \Delta d &= k_{d\varepsilon}\Delta\varepsilon + k_{dT}\Delta T \\ \Delta\lambda_B &= k_{\lambda\varepsilon}\Delta\varepsilon + k_{\lambda T}\Delta T \end{aligned}, \qquad (5)$$

where $k_{ij}$ are the measurand-induced responses of the sensors, with the subscripts $d$ and $\lambda$ denoting the FFI and FBG, respectively. Putting it into matrix form, inverting the sensitivity matrix (**K**), and solve for the measurand vector gives,

$$\begin{pmatrix} \Delta\varepsilon \\ \Delta T \end{pmatrix} = \frac{1}{\det(\mathbf{K})}\begin{pmatrix} k_{\lambda T} & -k_{dT} \\ -k_{\lambda\varepsilon} & k_{d\varepsilon} \end{pmatrix}\begin{pmatrix} \Delta d \\ \Delta\lambda_B \end{pmatrix}, \qquad (6)$$

with the condition that $\det(\mathbf{K}) = k_{d\varepsilon}k_{\lambda T} - k_{dT}k_{\lambda\varepsilon} \neq 0$. Thus, by knowing the ε and T induced responses of each sensor, simultaneous measurements can be performed.

## 4. EXPERIMENTS

### 4.1 Simultaneous measurement of ε and T

The demonstration of this demodulation technique is performed by measuring the ε and T of an aluminium (Al) plate. The setup is described in Subection 1.2. FBG was loosely attached onto the Al-plate, such that it was not affected by an applied strain field, i.e., $k_{\lambda\varepsilon} = 0$, while the FFI was adhered firmly next to the FBG using the superglue. After measuring the ε and T responses of both sensors, elements in the **K**-matrix are obtained: $k_{d\varepsilon} = 4.0558\times10^4$ pm/με, $k_{dT} = 1.1209\times10^6$ pm/°C and $k_{\lambda T} = 10.4$ pm/°C. Eq. (6) becomes,

$$\begin{pmatrix} \Delta\varepsilon \\ \Delta T \end{pmatrix} = \begin{pmatrix} 2.5\times10^{-5} & -2.7 \\ 0 & 9.6\times10^{-2} \end{pmatrix}\begin{pmatrix} \Delta d \\ \Delta\lambda_B \end{pmatrix}. \qquad (7)$$

The sensors were left in the laboratory overnight for a period of 14 hours, with no external ε applied. The FFI was subject to both thermal ε and T changes of the Al-plate, while the FBG was subject to T change only.

### 4.2 Crosstalk measurements

In another experiment, the crosstalk of the sensor system was investigated. Two FFIs and two FBGs were used, and only the ε measurement was considered. Since, the crosstalk between the same type of sensor is small, and is mainly due to the influence of different sensor types. Thus, the crosstalk between FBGs and FFIs were measured. An external ε was applied to each of the sensors while keeping other sensors free and unstrained, and their strain values were measured.

## 5. RESUTLS AND DISCUSSIONS

Figs. 3 (a) and (b) show the 3rd-level approximation coefficients for the FBG and the magnified view around the $\lambda_B$-peak, respectively. The coefficients give a smoothed and noise-reduced version of the original noisy signal. The $\lambda_B$-shift can be found directly from the coefficients. The measurement error (standard deviation) was ~2.0 pm and a resolution of ~1.2 pm after interpolation. Figs. 4 (a) and (b) show the 7th-level detail coefficients for the FFI, which is the interference pattern of the sensor, and the magnified FT magnitude spectrum of interference pattern around the peak, respectively. The $d$ can be determined directly from the magnitude spectrum. The measurement error was measured ~0.2 μm and a resolution of ~0.04 μm after interpolation.

The simultaneous and separate effects of thermal ε and T changes over the measurement period, using Eq. (7) and after further HT denoising, are shown in Fig. 5. Although both sensors experienced the same T change, the thermal ε did not correlate very well with the T change. This is because the FBG was loosely bonded onto the Al-plate, it was influenced by the surrounding T more than its thermal response. The local fluctuations were mainly due to environmental and human

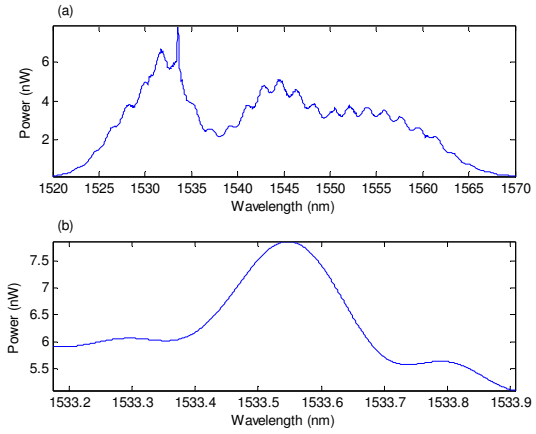


*Fig. 3. (a) 3rd-level approximation coefficients for the FBG; (b) magnification of (a) around the $\lambda_B$-peak.*

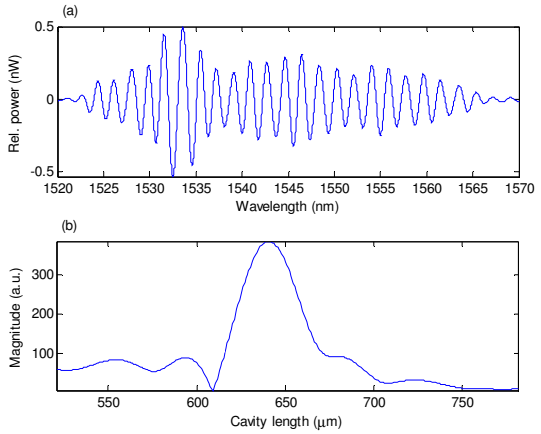


*Fig. 4. (a) 7th-level detail coefficients for the FFI; (b) magnified FT magnitude spectrum of (a) around peak.*

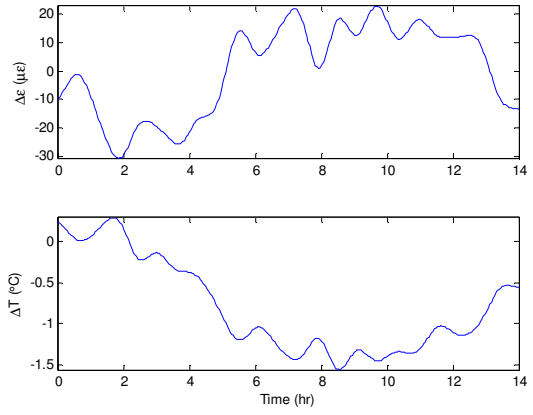


*Fig. 5. Simultaneous ε and T measurements for 14 hours.*

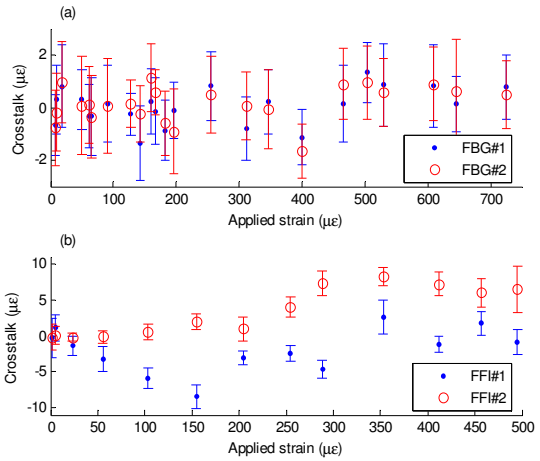


*Fig. 6. Crosstalk measurements of (a) FBGs due to FFIs, and (b) FFIs due to FBGs.*

perturbations, as well as equipment errors from light source fluctuations and OSA random jitters.

Fig. 6 shows the crosstalk measurements between FBGs and FFIs. There was no noticeable crosstalk (within error) of FBGs due to FFIs. There was a little crosstalk observed in FFIs due to FBGs, with a maximum of up to ~8.4 με, which was ~6 % of the applied ε values.

## 6. ACKNOWLEDGEMENTS

The authors thank Paul A. Childs for making FBG sensors, and Chris J.E. Phillips for helping in the signal processing. This work was supported in part by the Australian Research Council and the Roads and Traffic Authority, NSW, Australia, under a Linkage grant.

## 7. REFERENCES

[1] B. Lee, "Review of the present status of optical fiber sensors", Opt. Fiber Technol. **9**, pp57-79 (2003)

[2] G. Brady *et al* "Simultaneous interrogation of interferometric and Bragg grating sensors", Opt. Lett., **20**, pp1340-1342 (1995)

[3] J. Jiang *et al* "Parallel demodulation system and signal-processing method for extrinsic Fabry-Perot interferometer and fiber Bragg grating sensors", Opt. Lett., **30**, pp604-606 (2005)

[4] Y.J. Rao *et al*, "Spatial-frequency multiplexed fiber-optic Fizeau strain sensor system with optical amplification", Sens. Actuators A **120**, pp354-359 (2005)

[5] S.G. Mallet, "A theory for multiresolution signal decomposition: the wavelet representation", IEEE Trans. Pattern Anal. Machine Intell. **11**, pp674-693 (1989)

[6] D.L. Donoho and I.M. Johnstone, "Ideal spatial adaption by wavelet shrinkage", Biometrika **81**, pp425-455 (1994)

[7] T.T. Cai, "Adaptive wavelet estimation: a block thresholding and oracle inequality approach", Annals. Statist. **27**, pp898-924 (1999)